RECENT RESULTS FROM SLD

Mark Convery*
Stanford Linear Accelerator Center
Stanford University, Stanford, CA 94309

Representing the SLD Collaboration

ABSTRACT

New results from the SLD collaboration in the fields of electroweak, QCD and heavy flavor physics are presented. The analyses make use of all or part of SLD's final data sample of 550,000 Z^0 decays collected between 1993 and 1998. Many of the analyses exploit the large longitudinal polarization provided by the SLC's e^- beam. The precision vertexing provided by the CCD-based vertex detector is similarly key to many of the analyses.

Final results are presented for the total cross section asymmetry A_{LR}, the final state asymmetries A_c and A_s, and the B fragmentation function $D(x_B)$. Preliminary results are presented for A_b, for the final state branching ratios R_b and R_c and for B_s mixing.

*Supported by DOE Contract DE-AC03-76SF00515.

	SLC	LEP (Z^0 Running)
Center of Mass Energy	92 GeV	92 GeV
Circumference	3 km	27 km
Beam Size at IP	$3 \times 1\mu\mathrm{m}$	$400 \times 16\mu\mathrm{m}$
e^-/bunch	4×10^{10}	30×10^{10}
Crossing Rate	120 Hz	45 kHz
Z's/day/experiment	3000	30,000
e^- Polarization	0.75	0

Table 1. Table of beam parameters comparing SLC to LEP.

1 Introduction

The SLD experiment,[1] located at the interaction point of the Stanford Linear Collider (SLC), finished taking data at the Z^0 resonance in June of 1998. The total data sample taken in the years 1993 to 1998 consists of 550,000 Z decays. In this paper I will describe a number of analyses that have been performed using the SLD Data. These analyses cover topics in the fields of electroweak, QCD and heavy flavor physics. Many of them benefit from the unique beam conditions available at the SLC.

2 The Stanford Linear Collider (SLC)

The SLC, the world's first linear collider, produced Z^0 bosons by colliding electron and positron beams accelerated in the SLAC Linac. It ran between and 1989 and 1998 and by 1998, SLC's luminosity had improved to the point that it was producing 20,000 Z's per week of running. Table 1 compares the parameters of the SLC to those of CERN's Large Electron Positron Collider (LEP).

SLD is clearly at a statistical disadvantage to experiments running at LEP. However, in many cases, the advantages provided by the electron beam polarization - possible only at a linear collider, as well as the tiny beam spot of the SLC, can more than make up for the lower statistics.

fermion	$I^3_{L,f}$	Q_f	$g_{L,f}$	$g_{R,f}$	A_f	$\frac{\delta A_f}{\delta \sin^2_{\theta_W}}$
ν	1/2	0	0.5	0.0	1	0
e, μ, τ	-1/2	-1	-0.27	0.23	0.16	-7.9
u, c, t	1/2	2/3	-0.35	-0.15	0.69	-3.5
d, s, b	-1/2	-1/3	-0.42	0.07	0.94	-0.6

Table 2. Born Level couplings of the fermions to the Z.

3 Electroweak Asymmetries

The left- and right-handed couplings of the Z^0 to the various fermions at Born Level are given by

$$g_{L,f} = I^3_{L,f} - Q_f \sin^2 \theta_W^{eff} \quad (1)$$

$$g_{R,f} = Q_f \sin^2 \theta_W^{eff}, \quad (2)$$

where $I^3_{L,f}$ is the third component of weak isospin, Q_f is the charge of each fermion, and θ_w^{eff} is the *effective* value of the Weinberg angle at the Z^0.

This parity-violating difference in left- and right-handed coupling leads to a coupling asymmetry defined as

$$A_f \equiv \frac{g^2_{L,f} - g^2_{R,f}}{g^2_{L,f} + g^2_{R,f}} \quad (3)$$

Table 2 lists I^3_L, f, Q_f, $g_{L,f}$, $g_{R,f}$ and A_f for each of the fermions.

Expressed in terms of A_f, the differential cross-section for production of fermion pairs at the Z^0 is given by

$$\frac{d\sigma}{d\cos\theta_f} \sim (1 + P_e A_e)(1 + \cos^2\theta_f) + 2\cos\theta_f (A_e - P_e) A_f, \quad (4)$$

where θ_f is the dip angle of the final state fermion (not anti-fermion) and P_e is the longitudinal polarization of the incoming electron beam. From the first term, it is evident that there is a "production asymmetry" in the rate of Z^0 production for right-($P_e > 0$) and left-handed ($P_e < 0$) electrons. Clearly, it is necessary to have control of P_e in order to measure this asymmetry. Also, note that this production asymmetry is independent of final state. Therefore, it is not necessary to measure the type or charge of the final state fermions.

The second term in equation 4, since it is odd in $\cos\theta$, describes a forward-backward "decay asymmetry". To measure this asymmetry it is necessary to identify the type of fermions in the final state, as well as their charge. The asymmetry is present even if ($P_e = 0$), although it is enhanced if $P_e \neq 0$.

Experimentally, we define three observables that are sensitive to to A_f:

$$A^f_{FB} \equiv \frac{\sigma^f_F - \sigma^f_B}{\sigma^f_F + \sigma^f_B} = \frac{3}{4} A_e A_f \tag{5}$$

$$A_{LR} \equiv \frac{\sigma_L - \sigma_R}{\sigma_L + \sigma_R} = |P_e| A_e \tag{6}$$

$$A^f_{FB_{LR}} \equiv \frac{(\sigma^f_{FL} - \sigma^f_{BL}) - (\sigma^f_{FR} - \sigma^f_{BR})}{(\sigma^f_{FL} + \sigma^f_{BL}) + (\sigma^f_{FR} + \sigma^f_{BR})} = \frac{3}{4} |P_e| A_f, \tag{7}$$

where σ is the rate for $Z^0 \to hadrons$, σ^f is the rate for $Z^0 \to f\bar{f}$, "F" and "B" refer to forward ($\cos\theta_f > 0$) and backward ($\cos\theta_f < 0$) and "L" and "R" refer to left- and right-handed electron beams.

Equation 5 describes the unpolarized forward-backward asymmetry that can be measured even without electron polarization (e.g. at LEP). Equation 6 describes the production asymmetry that requires control of the electron polarization and is the most sensitive way to measure A_e at SLD. Equation 7 describes a polarization-enhanced forward-backward asymmetry that can be used to measure A_f for fermions other than electrons. The polarized asymmetries are useful both because they allow A_e and A_f to be measured independently and also because they give a large statistical enhancement of $(\frac{P_e}{A_e})^2 \approx 25$, which more than makes up for the factor 10 statistical advantage that LEP experiments have.

4 The SLD Detector

The SLD detector is a 4π multi-purpose detector that has many features in common with other e^+e^- detectors. Figure 1 shows a cutaway drawing of the SLD detector. Tracks emerging from the primary Interaction Point first pass through the precision vertex detector (called VXD3). They then pass through the Central Drift Chamber, where their momentum and direction are measured. They then enter the Cherenkov Ring Imaging Detector (called CRID), which is used to identify charged hadrons. A calorimeter made of lead and liquid argon (called the LAC) is used for photon energy measurements and electron identification. The Warm Iron Calorimeter (WIC) surrounds the detector and is used for muon identification and hadronic energy measurements. Also, a polarimeter based on Compton scattering is located just downstream of SLD and is used to measure

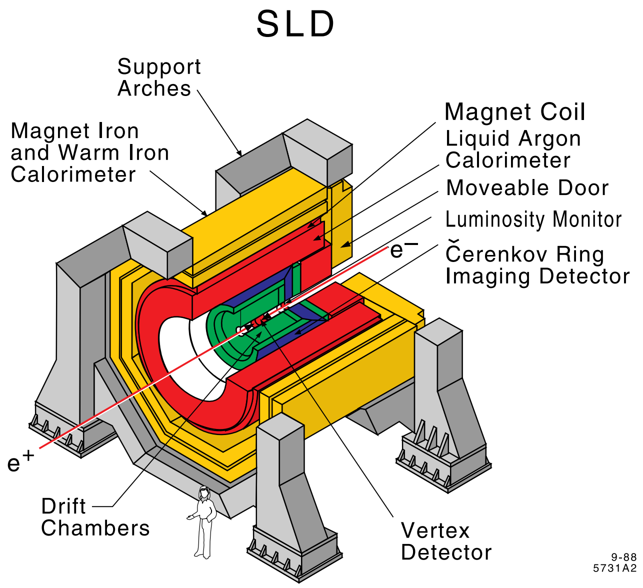

Fig. 1. Cutaway view of the SLD detector, located at the interaction point of the SLC.

the polarization of the electron beam. Since this polarimeter and the Vertex Detector are unique devices, they will be described in more detail in the following sections.

4.1 Vertex Detector

Since the SLC provides a very small and stable primary interaction point ($\sigma_{r\phi,measured} = 4\ \mu$m), it is desirable to have a vertex detector with similar resolution. This is provided by the upgraded vertex detector VXD3, which was installed in 1996. It is based on CCD technology and contains 307 million pixels. The achieved resolutions of this device are $\sigma_{r\phi} = 7.8\ \mu$m in the $r - \phi$ plane and $\sigma_{rz} = 9.8\ \mu$m in the $r - z$ plane. Topological vertexing and inclusive reconstruction algorithms exploit this excellent resolution.

4.2 Polarization Measurement

In order to exploit the electron beam polarization provided by the SLC, it is necessary to measure the average polarization, $\langle P_e \rangle$. This is done primarily with a Compton Polarimeter, shown in Figure 2. The counter collides the electron beam with a circularly polarized laser beam and measures the scattered electrons. Then, by measuring the Compton asymmetry, it is possible to extract the electron polarization. The counter can run during collisions so that P_e can be constantly monitored.

There are also two other counters, called the Quartz Fiber Calorimeter and Polarized

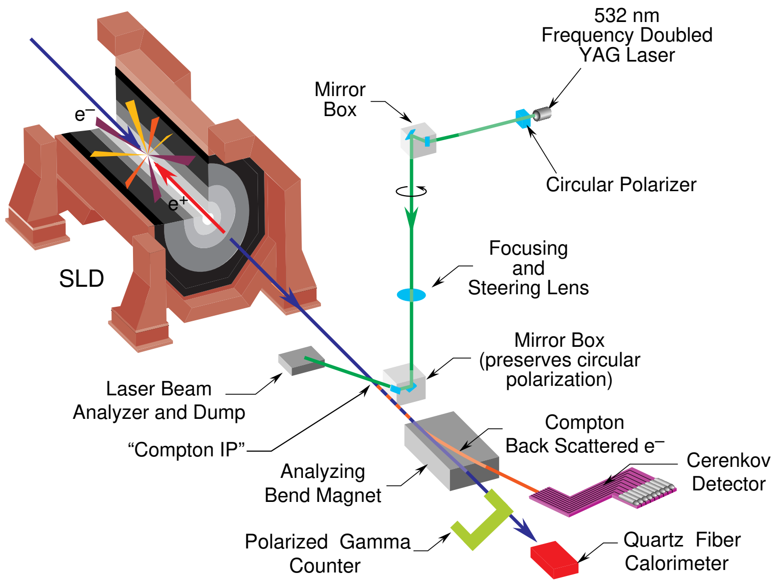

Fig. 2. Schematic of the electron polarization measuring devices located just downstream of the SLD.

Gamma Counter, which can only run during single beam running. These counters, however, provide a useful cross-check of the polarization measurement.

In '98 a separate test was performed to measure the polarization of the positron beam, which is not measured during colliding beam running and is normally assumed to be zero. The test found $P_{e^+} = -0.02 \pm 0.07\%$, which is so small as to be negligible in the electroweak measurements.

5 Electroweak Measurements

5.1 Measurement of A_{LR}

The measurement of A_{LR} is an extraordinarily simple and elegant one. All that it requires of from the SLD detector is a measurement of the number of $Z \to hadrons$ for left- and right-handed electrons. This leads to a cancellation of many possible systematic effects and hence a very small systematic error.

5.1.1 Experimental Corrections

The first step in the measurement of A_{LR} is the measurement of the raw asymmetry A_m, defined as:

$$A_m \equiv \frac{N_L - N_R}{N_L + N_R} \tag{8}$$

where N_L is the number of hadronic events produced with a left-handed electron beam N_R is the number produced with a right-handed beam.

To obtain the measurement of A_{LR} it is necessary to divide the raw asymmetry by the luminosity-averaged polarization of the electron beam ($\langle P_e \rangle$). This is defined as

$$\langle P_e \rangle = (1+\xi)\frac{1}{N_Z}\sum_{i=1}^{N_Z} P_i, \tag{9}$$

where P_i is the beam polarization at the time of production of the ith Z^0 and ξ is a factor that corrects for the difference in polarization between the Compton interaction point and the Z^0 production interaction point. ξ is found to be quite small ($\xi = 0.0012 \pm 0.0015$).

We can then calculate the value of A_{LR} at the beam energy as

$$A_{LR}(E_{beam}) = \frac{A_m}{\langle P_e \rangle}. \tag{10}$$

Since the SLC does not run exactly on the Z^0 pole, it is necessary to extrapolate to that energy and to correct for electroweak interference. These two corrections are treated together and parameterized by a single correction factor, ϵ:

$$A^0_{LR} = (1+\epsilon)A_{LR}(E_{beam}), \tag{11}$$

where A^0_{LR} is the inferred asymmetry at the Z^0 pole.

5.1.2 Systematic Errors

The systematic errors of the A_{LR} measurement come from uncertainties in the correction factors described in the previous section. Table 3 gives their numerical values. The largest systematics are related to the polarization measurement and to knowledge of the beam energy.

5.1.3 A_{LR} Result

Combining statistical and systematic errors, the final result on A_{LR}, using data taken between 1993 and 1998, is found to be $A^0_{LR} = 0.15138 \pm 0.00216$.[2] This corresponds to a measurement of $\sin^2\theta_W^{eff} = 0.23097 \pm 0.00027$. Clearly, the measurement is still statistically dominated. When combined with SLD's results on the leptonic coupling asymmetries,[3] the final value of $\sin^2\theta_W^{eff}$ is 0.23098 ± 0.00026.

Factor	Systematic Error
Polarization Measurement, $\langle P_e \rangle$	0.5%
Polarization Shift, ξ	0.15%
Experimental and Background Asymmetry	0.07%
Electroweak and Beam Energy Correction	0.39%
Total	0.65% ($\sigma_{syst}(A^0_{LR}) = 0.001$)

Table 3. Table of systematic errors for the A_{LR} measurement.

5.1.4 $\sin^2\theta_W^{eff}$ Comparisons

Figure 3 shows the world's measurements of $\sin^2\theta_W^{eff}$. The A_{LR} measurement has the lowest error. Since $\sin^2\theta_W^{eff}$ is sensitive to radiative corrections, it can be used in conjunction with the measured values of $\alpha(M_Z)$, G_F, M_Z and M_t to measure the Higgs Mass (m_H). See section 5.5 for more details on this.

5.2 Measurement of R_b

Measurements of R_b and R_c ($R_q \equiv \frac{\Gamma(Z\to q\bar{q})}{\Gamma(Z\to hadrons)}$) are also performed at SLD.

5.2.1 Radiative Corrections to R_b

Measurements of R_b are especially interesting because of its sensitivity to vertex corrections such as the one shown in Figure 4. In the Standard Model, the top quark diagram changes the value of R_b by:

$$\delta_{R_b} \approx -\frac{20}{13}\frac{\alpha}{\pi}\left[\frac{M_t^2}{M_Z^2} + \frac{13}{6}\ln\frac{M_t^2}{M_Z^2}\right] \approx -0.025. \tag{12}$$

Other new physics may change the value of R_b by similar amounts and so precision measurements of R_b become very interesting.

5.2.2 Inclusive b and c Reconstruction

The first step in measuring R_b and R_c is developing a highly pure and efficient method of tagging event hemispheres that contain b or c quarks. At SLD, this is done using an inclusive reconstruction technique. Figure 5 illustrates this technique. After splitting the event into hemispheres, the technique selects tracks that are considered to have

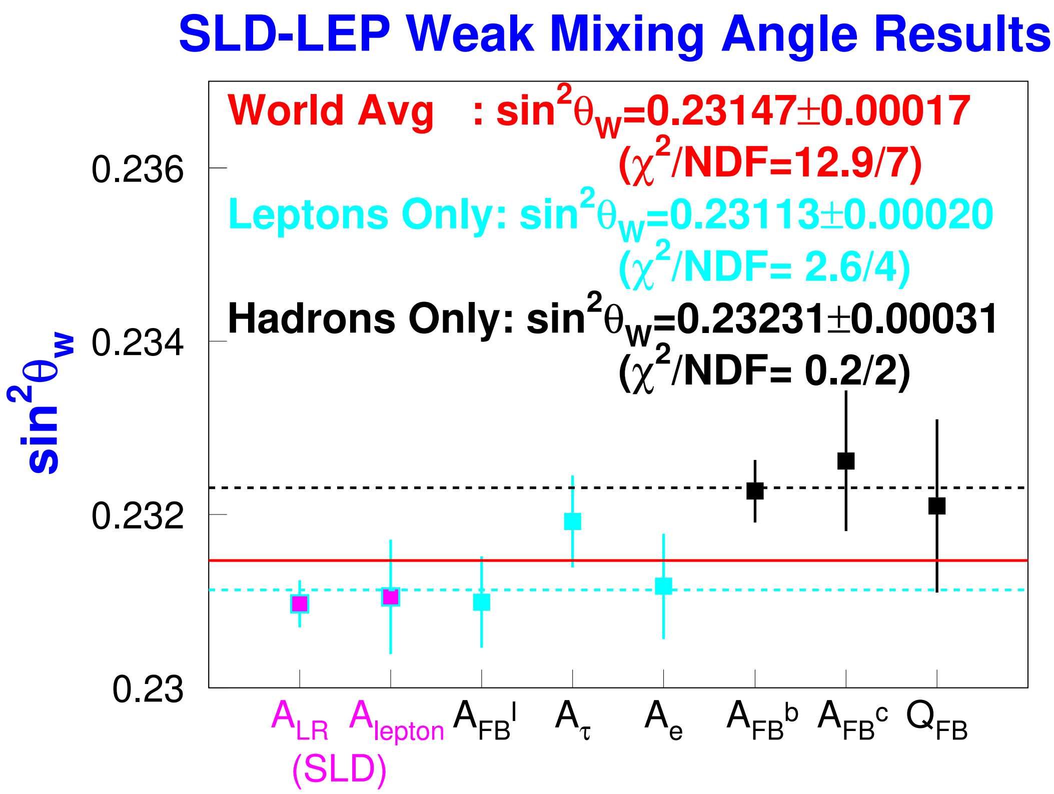

Fig. 3. The world's measurements of $\sin^2\theta_W^{eff}$ at the Z^0 pole.

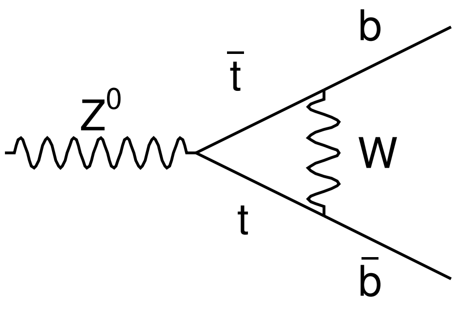

Fig. 4. The Feynman diagram for a Standard Model radiative correction to R_b. New physics may couple in a similar way.

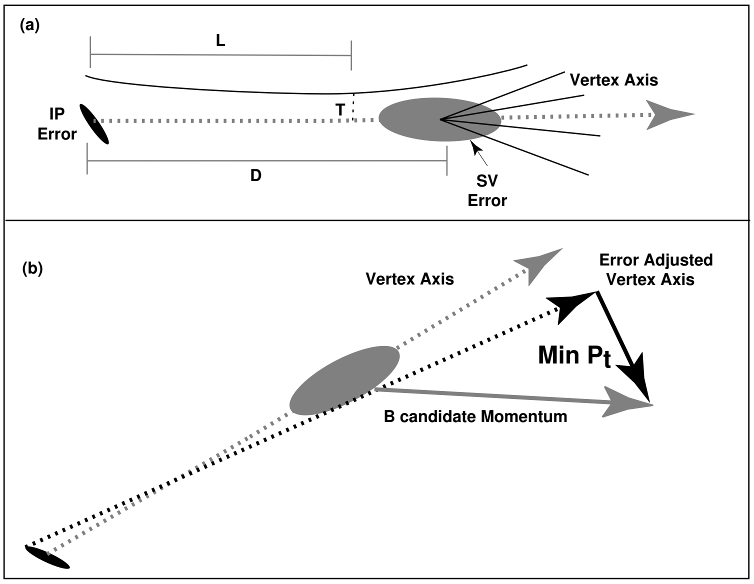

Fig. 5. Illustration of the inclusive b and c reconstruction technique. In (a), a seed vertex (SV) is topologically identified and tracks are attached to it based on their values of L, T and D. In (b), the calculation of M_{pt} is demonstrated.

come from the b or c quark. This is done by topologically identifying a "seed" vertex (as shown in Figure 5(a)) in each hemisphere.[4] Due to the finite charm lifetime, not all of the tracks coming from the b decay are expected to come from a single point. Therefore, a "track attachment" algorithm is needed to attach tracks to this seed vertex. A neural net based on the variables T, L and D as defined in Figure 5(a) is used to perform this attachment. Roughly speaking, tracks with $T < 1\,\mathrm{mm}$, $L > 0.5\,\mathrm{mm}$ and $L/D > 0.25$ are attached to the vertex.

Then, the mass (M_{raw}) of this set of "b-tracks" is calculated under the assumption that each track is a pion. To correct for the effect of missing tracks and neutrals, a "P_t corrected mass" is calculated as:

$$M_{pt} = \sqrt{M_{raw}^2 + P_t^2} + |P_t|, \tag{13}$$

where P_t is the momentum of the b-tracks transverse to the flight direction. This flight direction is chosen so as to minimize the P_t within one-sigma vertex errors, as shown in figure 5(b). Figure 6(a) shows a plot of M_{pt} for Monte Carlo and data. Clearly, there is good separation between b, c and uds quarks in this variable alone. In the Monte Carlo, cutting at $M_{pt} > 2$ GeV gives a b purity of 98% and a b efficiency, $\epsilon_{b\to b}$, of 57%.

A Neural Net based on M_{pt} and other related variables is used to improve the ef-

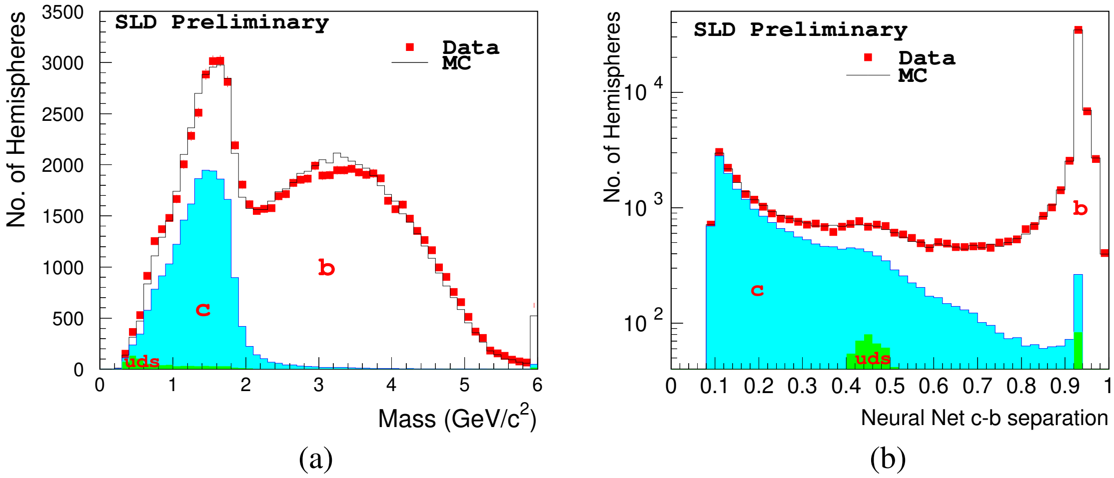

Fig. 6. (a) shows the distribution of M_{pt} in data and for Monte Carlo. (b) shows the output of the Neural Net based on M_{pt} and other related quantities. The output is close to zero for c quarks and close to one for b quarks.

ficiency of the b-tag. Figure 6(b) shows the output of the neural net, which is ideally close to one for b hemispheres and close to zero for c hemispheres. Figure 7 shows the efficiency and purity of a b-tag based on this neural net as a function of the cut position. At a cut position of 0.75, the efficiency is improved to 63% while maintaining a purity of 98%.

5.2.3 Double Tag Method

In order to measure R_b, it is necessary to know the efficiency of the single hemisphere b-tag ($\epsilon_{b\to b}$). To measure $\epsilon_{b\to b}$, and hence R_b, with the lowest possible systematic error, we use a "double tag method". This allows us, essentially, to measure $\epsilon_{b\to b}$ in data without relying on Monte Carlo. This reduces possible systematic errors due to lack of knowledge of the b production spectrum (fragmentation function), b decay modeling and detector modeling.

In the limit that the mistagging of charm ($\epsilon_{c\to b}$) and light quarks ($\epsilon_{uds\to b}$) are both zero, and that there are no hemisphere correlations, we can write the the efficiency of the b-tag as

$$\epsilon_{b\to b} = 2\frac{N_{double}}{N_{hemi}}, \tag{14}$$

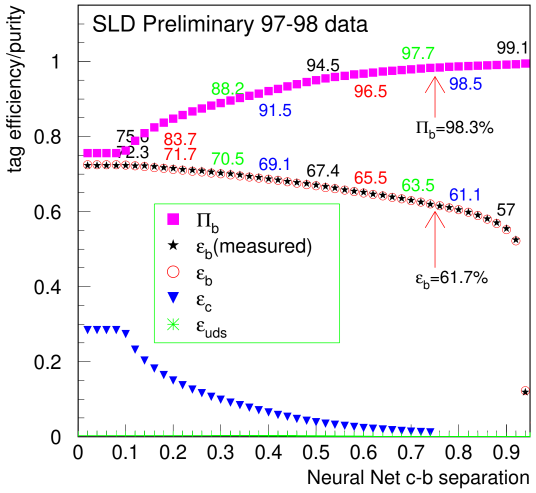

Fig. 7. Efficiency (ϵ_b) and purity (π_b) for b tagging as a function of the cut position on the Neural Net output.

Factor	Systematic Error
Running b mass	0.00067
Tracking	0.00041
D Modeling	0.00042
Total	0.00094

Table 4. Table of the largest systematic errors for the R_b. Several other smaller contributions are included in the total.

where N_{double} is the number of events with two tagged hemispheres and N_{hemi} is the number of tagged hemispheres. Knowing $\epsilon_{b\to b}$, the calculation of R_b is straightforward.

In the actual measurement, the Monte Carlo is used to make corrections for mistagging and for hemisphere correlations.

5.2.4 R_b Result

Figure 8 shows the measured value R_b for a range of values of the cut on the output of the Neural Net. The stability of the measurement gives us confidence that the Neural Net output is well understood. Table 4 lists the largest of the systematics involved in the measurement.

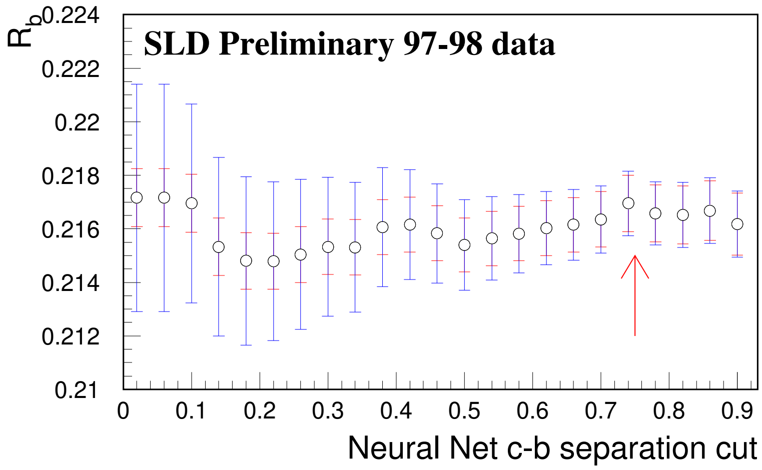

Fig. 8. Measured value of R_b as a function of the Neural Net cut.

The preliminary result using data taken from '93 to '98 is $R_b = 0.21669 \pm 0.00094_{stat} \pm 0.00101_{syst}$. This is to be compared to the world average as of Summer 2000 — $R_b = 0.21653 \pm 0.00069$ and the Standard Model value of 0.2157.[5]

5.3 R_c Measurement

The measurement of R_c is quite similar to R_b. As shown in Figure 6(b), the same Neural Net that is used for b-tagging can also be used for charm tagging. This tag has an efficiency for correctly tagging charm quark jets of $\epsilon_{c\rightarrow c} = 17.4\%$, and a purity of $\pi_{c\rightarrow c} = 84.5\%$ at the nominal cut position. Figure 9 shows the efficiency and purity as a function of cut position. Also, a double tag technique is used to minimize the systematic errors.

The largest systematics of the measurement are related to charm decay modeling ($\delta R_c = 0.0017$) and Interaction Point correlations ($\delta R_c = 0.00116$). The preliminary result based on data taken between '96 and '98 is $R_c = 0.1732 \pm 0.0041_{stat} \pm 0.0025_{syst}$. This is to be compared to the world average as of Summer 2000 of $R_c = 0.1709 \pm 0.0034$ and the Standard Model value of 0.1725.[5]

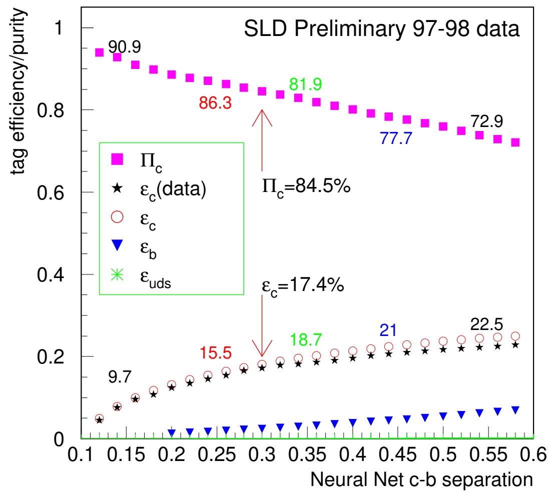

Fig. 9. Efficiency (ϵ_c) and purity (π_c) for $c-$tagging as a function of the cut on the Neural Net Output.

5.4 Measurement of A_b, A_c and A_s

The measurement of the quark asymmetries takes advantage of the polarized cross-section for quark production:

$$\frac{d\sigma}{d\cos\theta_f} \sim (1 + P_e A_e)(1 + \cos^2\theta_f) + 2\cos\theta_f(A_e - P_e)A_f, \tag{15}$$

where θ_f is the dip angle of the final state fermion (not anti-fermion) and P_e is the polarization of the electron beam. Therefore, to measure the quark asymmetries, we need to be able to tag not only the *quark flavor* (u, d, s, c, b), but also the *quark charge* (*e.g.* b or $\bar{b}$). For A_b and A_c, SLD has developed a number of techniques for tagging quark flavor. In this paper, we will cover only those with recent new results.

5.4.1 A_b with Lepton Tag

This analysis begins by identifying hemispheres with with b or $\bar{b}$ quarks using the Neural Net Mass Tag described in section 5.2.2. Then, it uses identified muons and electrons among the vertex tracks to tag the quark charge via the decay $b \to l$. The largest background to this process is the cascade decay $b \to c \to \bar{l}$, which produces oppositely charged leptons and thus incorrect tags. These cascade decays can be distinguished from the direct ones by examining their total momentum (p), their momentum trans-

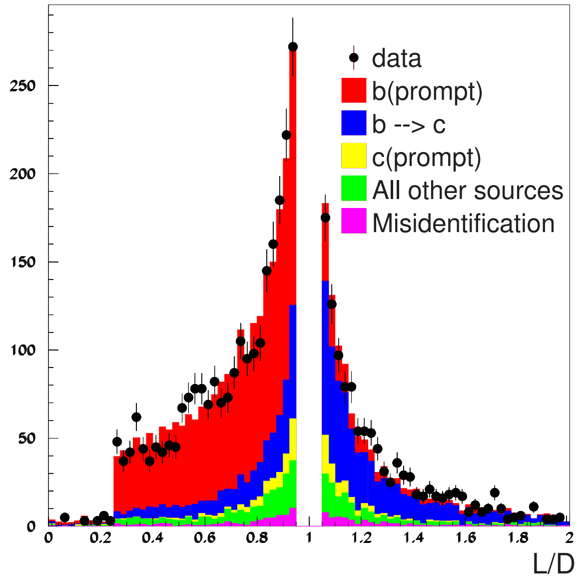

Fig. 10. Distribution of $\frac{L}{D}$, as defined in Figure 5, for direct (prompt) and cascade leptons.

verse to the the jet direction (p_t) and by using vertexing information. The vertexing information is incorporated by noting that leptons coming from direct $b \to l$ decays should tend to come from closer to the primary vertex, whereas those coming from cascade decays should come from farther away. In terms of the variables defined in Figure 5(a), this means that direct decays should have $L/D < 1$ and cascade decays should have $L/D > 1$. Figure 10 shows the Monte Carlo distributions of L/D for direct and cascade decays. Clearly, there is good separation in this variable.

A Neural Net is used to combine the three types of information used in the tagging. Figure 11 shows the output of this Neural Net, which returns values close to one for direct leptons and close to zero for cascade.

Using this tag, the preliminary result for data taken between '93 and '98 is[6] $A_b = 0.922 \pm 0.029_{stat} \pm 0.024_{syst}$.

5.4.2 A_b with Vertex Charge

An alternative method of tagging the quark charge is to use the total charge of the tracks associated to the b-vertex as described in section 5.2.2. Clearly, this method will work only for charged b-hadrons. To improve the charge reconstruction, tracks which were found in the Vertex Detector, but not in the drift chamber are included in the charge calculation. Figure 12 shows how the charge purity is improved by using these tracks.

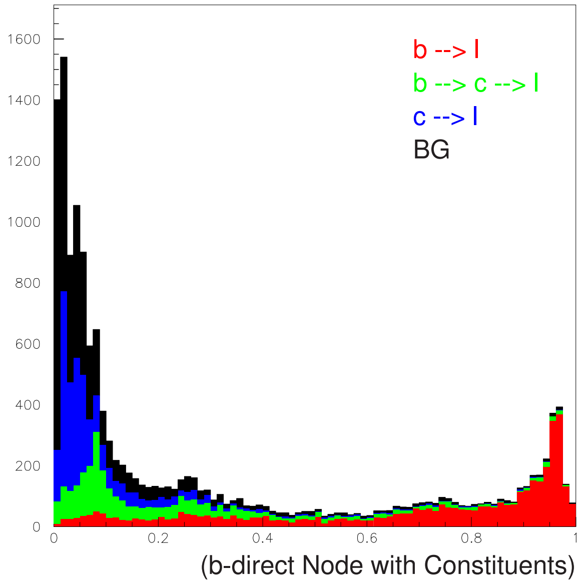

Fig. 11. Output of the Neural Net used for distinguishing direct and cascade leptons.

The analyzing power is improved from 0.58 to 0.64.

Figure 13 shows the asymmetry separately for left and right handed polarized electron beams. The preliminary result based on data taken between '97 and '98 is[7] $A_b = 0.926 \pm 0.019_{stat} \pm 0.027_{syst}$.

5.4.3 A_b Combined Average

Combining A_b measured with the lepton tag and with the vertex charge tag, along with two other SLD measurements based on a Kaon tag and on a jet charge tag, we find an SLD average of $A_b = 0.914 \pm 0.024$. This is to be compared with the the LEP average as of Summer 2000 of 0.880 ± 0.020 and the Standard Model value of 0.926.[5]

5.4.4 Measurement of A_c Using Exclusive Reconstruction

The most straightforward way to measure A_c is by directly reconstructing the charmed mesons produced. In the SLD analysis, we reconstruct D decays in the following exclusive modes (and their charge conjugates):

- $D^{*+} \to D^0\pi^+(D^0 \to K^-\pi^+)$
- $D^{*+} \to D^0\pi^+(D^0 \to K^-\pi^+\pi^0)$
- $D^{*+} \to D^0\pi^+(D^0 \to K^-\pi^+\pi^+\pi^-)$

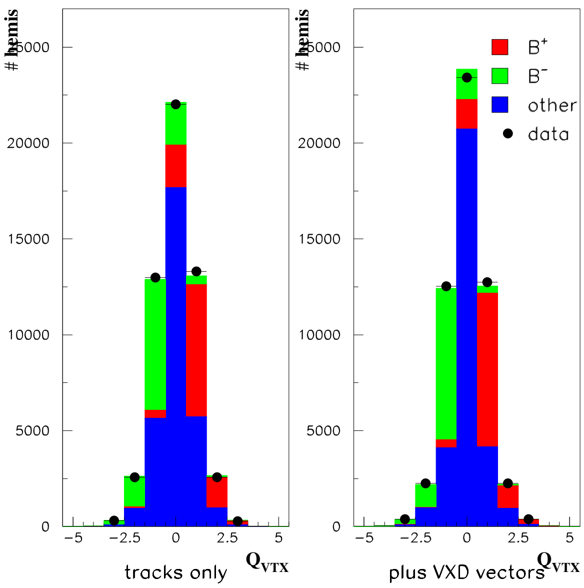

Fig. 12. (a) shows the vertex charge when using only tracks reconstructed in the vertex detector *and* the Drift Chamber. (b) shows the same quantity when tracks reconstructed only in the vertex detector are included.

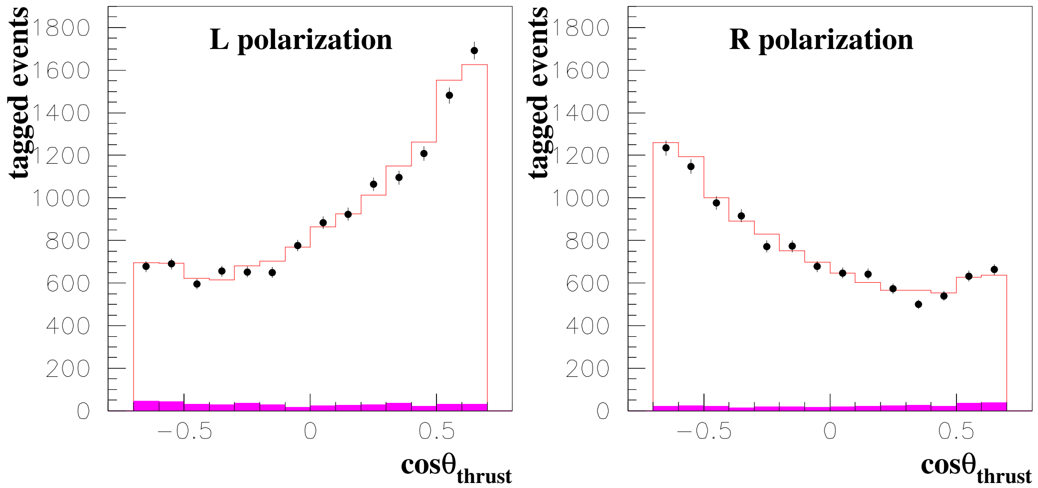

Fig. 13. The b-production asymmetry using a vertex charge tag shown separately for left- and right- electron polarizations.

- $D^{*+} \to D^0\pi^+(D^0 \to K^- l^+ \nu)$
- $D^+ \to K^-\pi^+\pi^-$
- $D^0 \to K^-\pi^+$

Figure 14 shows plots of $\Delta m \equiv m_{D^{*+}} - m_{D^0}$ for each of the D^{*+} modes. A clear signal is seen for each mode.

A large background that needs to be rejected in this analysis is D mesons coming from $b \to c$ decays. These can be rejected by requiring that the D come directly from the primary interaction point, and by applying a b-veto to the opposite hemisphere.

The final result from this analysis for data taken between '93 and '98 is $A_c = 0.690 \pm 0.042_{stat} \pm 0.021_{syst}$.[8]

Combining this result with other SLD results based on leptons, on inclusive reconstruction with Kaon and vertex charge tagging and of a soft π^+ tag, we find an SLD average result of $A_c = 0.635 \pm 0.027$. This is to be compared with the LEP average of $A_c = 0.612 \pm 0.032$ and the Standard Model value of 0.675.[5]

5.4.5 Measurement of A_s

The measurement of A_s relies on the QCD "Leading Particle" effect, which predicts that very high momentum kaons will come preferentially from $Z \to s\bar{s}$ decays. The analysis uses identified $K^{\pm}$'s with $p > 9$ GeV, which are 92% pure, and K_s^0's with $p > 5$ GeV, which are 91% pure. Events with either a K^+K^- combination, or a $K^{\pm}K_s^0$ combination are selected. In the Monte Carlo, 66% of these events are $Z^0 \to s\bar{s}$ and they have an 82% analyzing power.

Figure 15 shows the asymmetry separately for left and right handed electron polarizations. The final result for data taken between '93 and '98 is[9] $A_s = 0.895 \pm 0.066_{stat} \pm 0.062_{syst}$.

5.5 Global Electroweak Comparison

The consistency of the world's measurements of electroweak parameters with the Standard Model can be checked in Figure 16. The SLD measurement of A_b is consistent with the Standard Model. The LEP measurement of A_{FB}^b seems to favor a heavy Higgs. The "orthogonality" of SLD's measurements of A_{LR} and A_b is clearly useful because it minimizes the area of the overlap region between them.

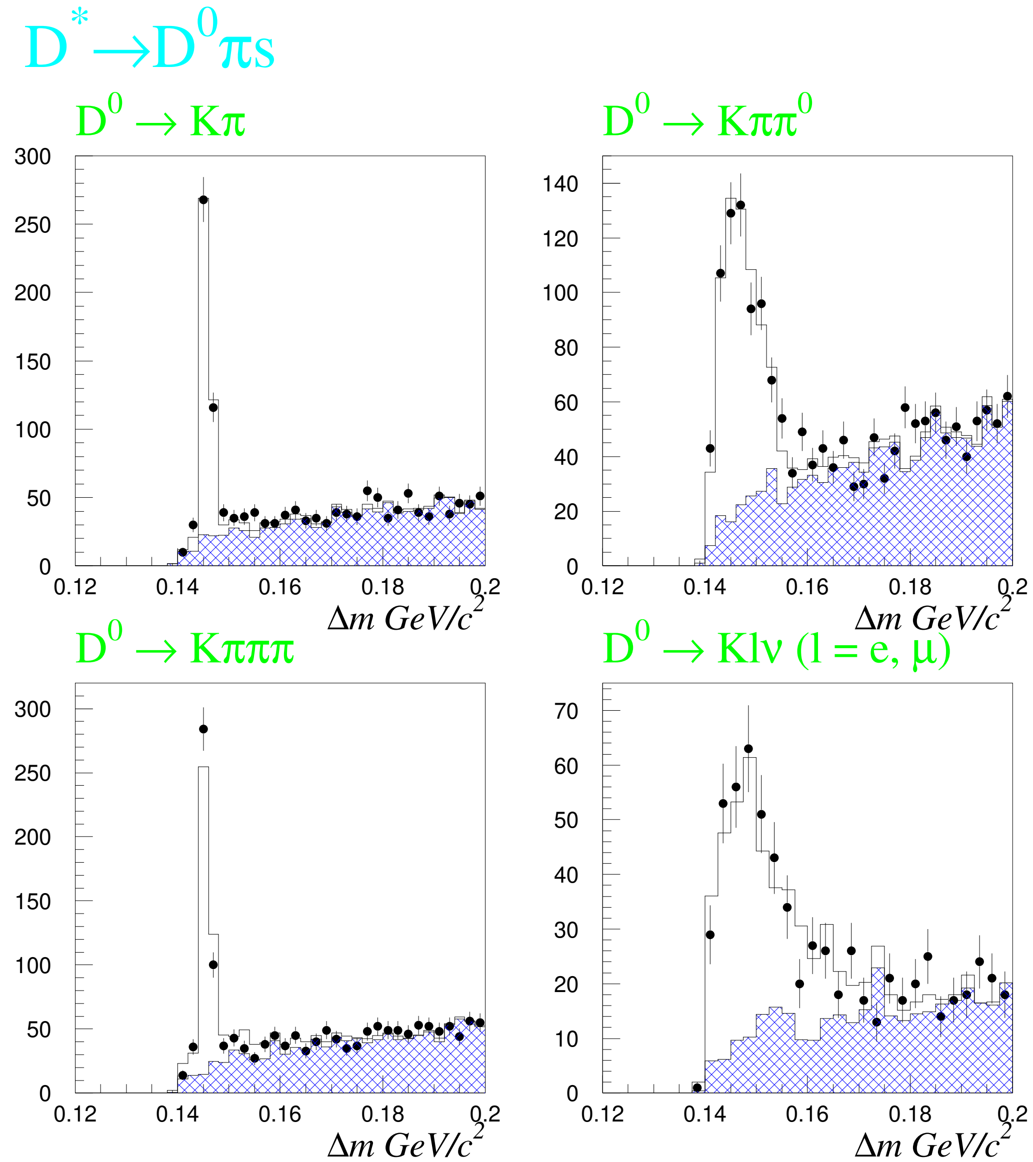

Fig. 14. Plots of Δm for each of the D^{*+} modes reconstructed in the A_c analysis. Clear signals are seen in each mode.

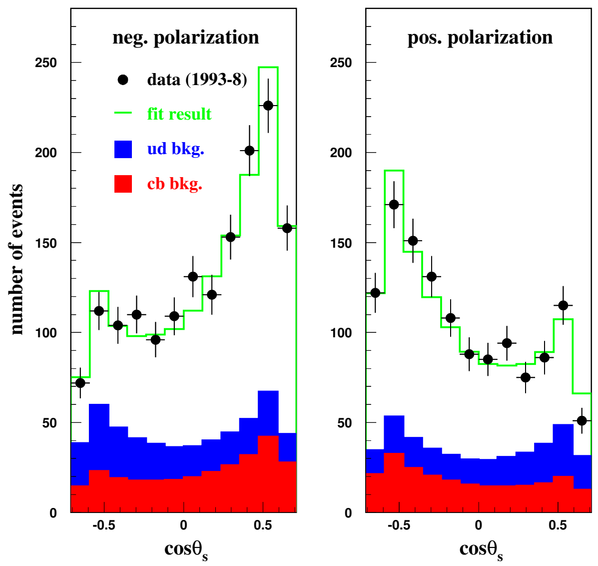

Fig. 15. The s-quark production asymmetry shown separately for left (negative) and right (positive) polarizations.

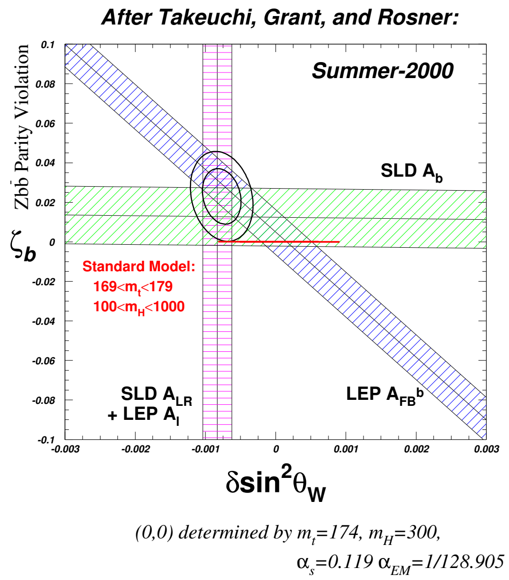

Fig. 16. A check for consistency with the Standard Model of the world's electroweak measurements. The Standard Model lies on a line at $\xi_b = 0$ between $\delta \sin^2 \theta_w \approx -0.001$ and $\delta \sin^2 \theta_w \approx 0.001$

Alternatively, one can use the various electroweak measurements to calculate the Higgs mass within the Standard Model. Figure 17 shows the Higgs mass limits that can be extracted from each of the electroweak measurements. A very tight limit ($m_H <$

147 GeV at 95% confidence) can be extracted from the SLD measurement of $\sin^2\theta_W^{eff}$ alone. All measurements except A^b_{FB} favor a light Higgs mass.

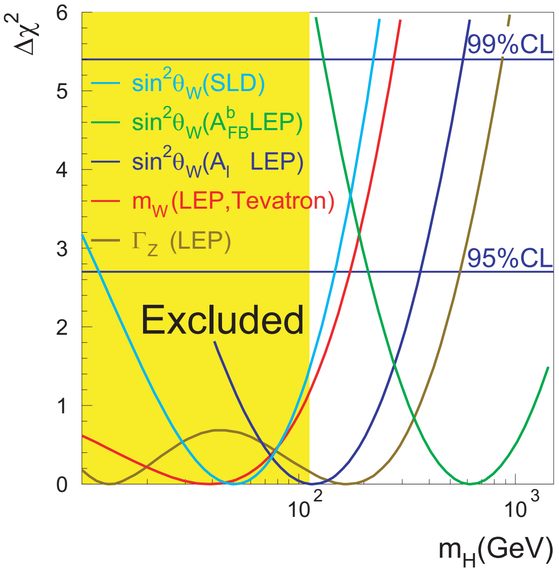

Fig. 17. Using different measurements of $\sin^2\theta_w^{eff}$ to constrain the Higgs Mass. SLD's measurements provide the single tightest limit.

6 Measurement of the B Fragmentation Function

The measurement of the B hadron production spectrum $D(x_B)$, where $x_B \equiv E_b/E_{beam}$, which is called the B Fragmentation Function, is interesting for a number of reasons. It can give useful input to B physics analysis, since $\langle x_B \rangle$ is often a large systematic. Also, it may help in the understanding of the rate of $b\bar{b}$ production in $p\bar{p}$ collisions, which is twice as large as predictions. Finally, it is a good place to test Heavy Quark Effective Theory (HQET).

6.1 x_B Reconstruction

The SLD analysis performs an inclusive reconstruction of x_B based solely on charged tracks.[10] The analysis begins the same as the inclusive B reconstruction algorithm described in section 5.2.2. As shown in Figure 18, the composite system of measured tracks has total momentum (p_{ch}) transverse momentum (p_T) and longitudinal momentum (p_L) defined relative to the vertex direction. The algorithm then defines a "missing system" whose p_T is equal and opposite to that of the measured system, and whose mass, m_0, and longitudinal momentum p_{0L} are unknown. We can, however, place a limit on m_0 by noting that, in the B rest frame,

$$m_B = \sqrt{m_{ch}^2 + p_T^2 + p_L^2} + \sqrt{m_0^2 + p_T^2 + p_L^2}. \tag{16}$$

So,

$$m_B \geq \sqrt{m_{ch}^2 + p_T^2} + \sqrt{m_{ch}^2 + p_T^2}. \tag{17}$$

Therefore, noting that p_T is a Lorentz invariant, we can set a limit,

$$m_0^2 < m_{0,max}^2 \equiv m_B^2 + m_{ch}^2 - 2m_B\sqrt{m_{ch}^2 + p_T^2}. \tag{18}$$

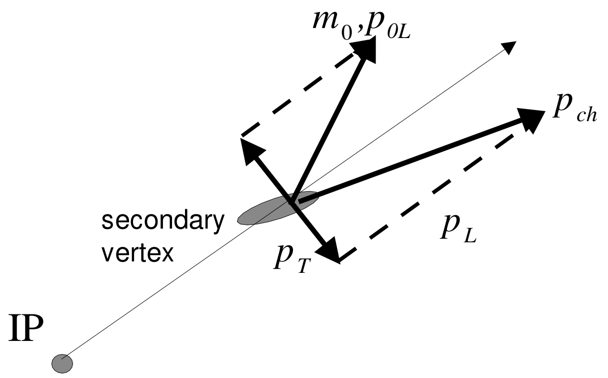

Fig. 18. Illustration of the variables used in the inclusive x_B reconstruction procedure.

Then, if we select hemispheres with small $m_{0,max}^2$, we preferentially select those hemispheres that are close to being fully reconstructed and therefore are measured with good energy resolution. We then set $m_0 = m_{0,max}$ and calculate x_B. Figure 19(a) shows the efficiency of this procedure and 19(b) shows the fractional energy resolution that is achieved.

6.2 Data/Monte Carlo Comparison

Figure 20 shows the results of applying this x_B reconstruction to the data and comparing to Monte Carlo, which was generated with the Jetset program.[11] Clearly, there is a discrepancy between the two.

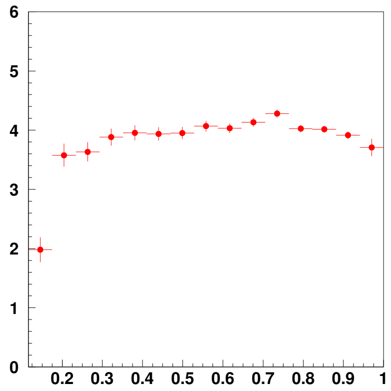

(a)

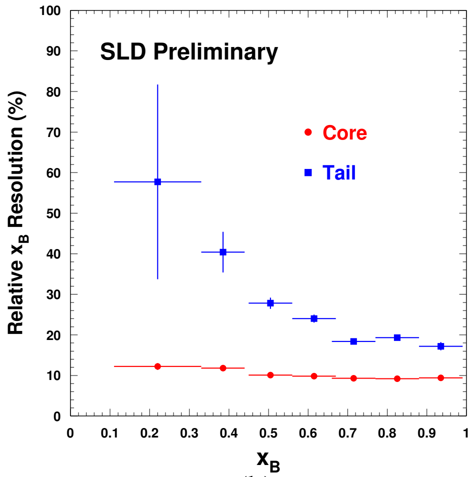

(b)

Fig. 19. (a) shows the efficiency for of the x_B reconstruction procedure as a function of x_B. (b) shows the x_B resolution achieved as as a function of x_B.

6.3 Unfolding and $\langle x_B \rangle$

Ideally, we would like to take out the effects of resolution in order to produce the parent distribution. This "unfolding" procedure is complicated, however, because it depends on the fragmentation model that is used. This model dependence can be reduced by using a procedure called, "Singular Value Decomposition with Regularization".[12] Figure 21 shows the unfolded spectrum that is obtained with this procedure.

We can also extract the average B energy, $\langle x_B \rangle$. The final result based on data taken between '97 and '98 is $\langle x_B \rangle = 0.709 \pm 0.003_{stat} \pm 0.005_{syst}$.

7 Measurement of B_s^0 Mixing

As shown in Figure 22, B_s mixing is very similar to the more familiar B_d mixing. B_d mixing has been rather precisely measured, with a world average value of $\Delta m_d = 0.472 \pm 0.016$ ps^{-1}. B_d mixing is interesting because it is sensitive to the CKM parameter[13] V_{td}

$$\Delta m_d \propto m_{B_d} f_{B_d}^2 B_{B_{B_d}} \eta_{QCD} |V_{tb}^* V_{td}|^2, \tag{19}$$

where m_{B_d} is the mass of the B_d meson, $f_{B_d}^2$ and $B_{B_{B_d}}$ are QCD-related factors that need to be calculated and η_{QCD} is a QCD correction factor that is well known. Naively,

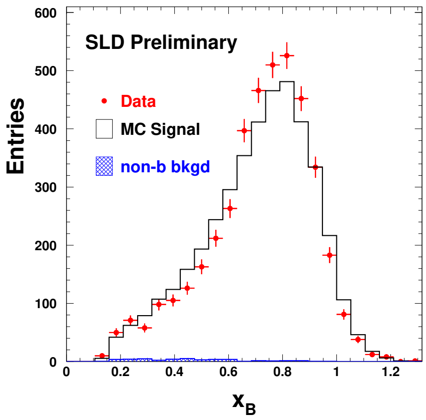

Fig. 20. The B fragmentation function $D(x_B)$ as measured in data compared to Monte Carlo.

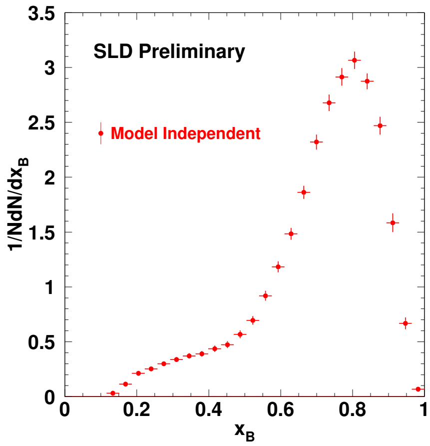

Fig. 21. The "unfolded" $D(x_B)$ spectrum, which has had efficiency and resolution effects removed in a model independent manner.

one might think that one could use the measured value of Δm_{B_d} to measure V_{td}. However, this is complicated because the hadronic factor, $f_{B_d}\sqrt{B_d}$ is not well known. The theoretical estimate is[13]

$$f_{B_d}\sqrt{B_d} = 201 \pm 42 \text{ MeV}. \tag{20}$$

This uncertainty spoils any estimate of V_{td} based on B_d mixing.

B_s mixing provides a way around this uncertainty. As can be seen in Figure 22, the only major difference is that rather than having a factor of V_{td} at the vertices, B_s mixing

Fig. 22. Feynman diagrams for B_d and B_s mixing.

has V_{ts}. The expression for Δm_s is therefore,

$$\Delta m_s = m_{B_s} f_{B_s}^2 B_{B_s} \eta_{QCD} |V_{tb}^* V_{ts}|^2, \tag{21}$$

where the factors are all similar to those for B_d. Since V_{ts} is much greater than V_{td}, we expect B_s mixing to be roughly 15 times faster than B_d mixing. Now, if one takes the ratio $\frac{\Delta m_s}{\Delta m_d}$, many of the theoretical uncertainties cancel and one is left with

$$\frac{\Delta m_s}{\Delta m_d} = \frac{m_{B_s} f_{B_s}^2 B_{B_s}}{m_{B_d} f_{B_d}^2 B_{B_s d}} \left|\frac{V_{ts}}{V_{td}}\right|^2 = (1.11 \pm 0.06) \left|\frac{V_{ts}}{V_{td}}\right|^2. \tag{22}$$

So, by measuring B_s mixing, we can turn B_d^0 mixing into a precision measurement of V_{td}.

7.1 Ingredients

Since B_s mixing is so fast, it is necessary to do time dependent measurements. To do so requires three ingredients.

- Initial State Tag: Determine quark-charge of B_s^0 at the time of production.
- Final State Tag: Determine quark-charge of B_s^0 at the time of decay.
- Proper time of the B_s^0 decay: Requires measurement of decay length and boost of the B_s^0.

The "Moser Formula" for B_s^0 mixing significance[14] is a convenient way of demonstrating the importance of each of these components. It reads:

$$S = \sqrt{\frac{N}{2}} f_{B_s} (1 - 2w) e^{-\frac{1}{2}(\Delta m_s \sigma_t)^2}, \tag{23}$$

where S is the expected significance of a Δm_s measurement, N is the number B_s^0 candidates identified, f_{B_s} is the B_s^0 purity, w is the quark charge mistag rate, and σ_t is the proper time resolution. σ_t can be written as the sum of two terms,

$$\sigma_t^2 = \left(\frac{\sigma_L}{\gamma\beta c}\right)^2 + \left(\frac{\sigma_p}{p}t\right)^2, \tag{24}$$

where σ_L is the decay length resolution, p, γ and β are the usual kinematic variables for the B_s. From equation 23 it is clear that while purity and tagging are important, it is absolutely essential to have excellent proper time resolution. This is because for $\Delta m_s > 10$ ps^{-1}, the significance will be exponentially damped unless $\sigma_t < 0.1$ ps. Since γ is typically 5 at the Z^0 pole the decay length resolution needs to be of order 100 μm or better. SLD's excellent vertex resolution yields excellent σ_t resolution, which makes SLD's measurements competitive at high Δm_s, even with lower statistics than LEP.

The following sections will describe each of the three ingredients in turn.

7.2 Initial State Tag

The initial state tag takes advantage of the forward-backward asymmetry of B mesons produced in Z^0 decay. This asymmetry is enhanced by the polarization of the SLC electron beam. Figure 23 shows the polar angle of b quarks (not $\bar{b}$) produced with left- and right-handed electron beams. Using the polarization as an initial state tag is 100% efficient (since the polarization is known for every event), and provides the correct tag 72% of the time. In order to enhance the initial state tag, information from the b-decay on the "opposite side" is also used. This information includes the jet charge, the vertex charge, the charge of any kaons, the charge of any leptons and the "dipole", which is described in section 7.3.3. This combined tag has a 75 to 78% correct tag probability. Figure 24 shows the output of this tag.

7.3 Final State Tags

The final state tag must identify the quark charge of the B_s^0 (i.e. b or $\bar{b}$) and provide a way to measure the time of the decay. A number of different techniques are used to provide this tag. The quality of each technique is parameterized by its B_s purity (f_{B_s}), its boost resolution ($\frac{\sigma_p}{p}$), its quark charge mis-tag fraction (w_{final}), and its decay length resolution (σ_L), which is calculated from a double gaussian fit with a fixed "core" frac-

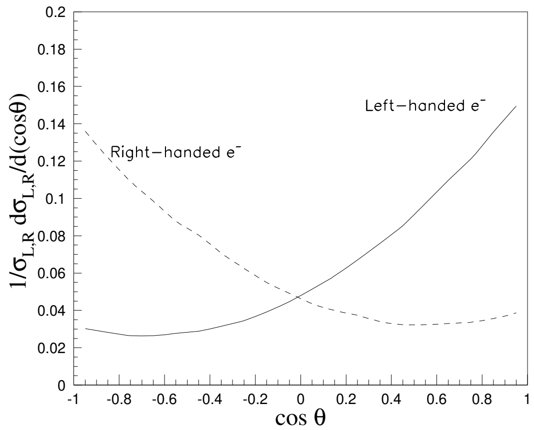

Fig. 23. Polar angle distribution for b-quarks produced at the Z^0, shown separately for right- and left-handed electron beams.

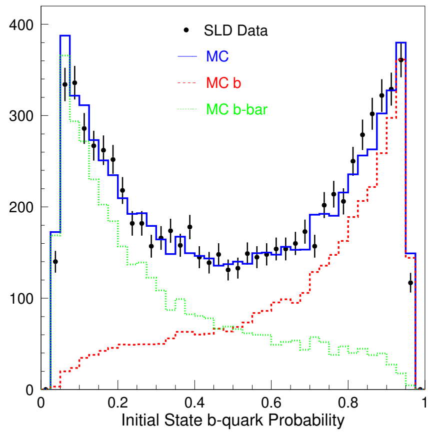

Fig. 24. Distribution of the computed initial state b-quark probability.

tion of 60%. Table 5 lists these parameters for each tagging technique. The following sections describe each tag in more detail.

7.3.1 D_s + Tracks

In the "D_s + Tracks" method, a D_s meson is exclusively reconstructed through either $D_s^- \to \phi\pi^-$ or $D_s \to K^{*0}K^-$. Identifying the charged kaons with the CRID greatly reduces the combinatoric background. The trajectory of the reconstructed D_s is then intersected with the other tracks of the vertex to form the B decay vertex, from which h

Tagging Technique	f_{B_s}	σ_L (60% Core)	$\frac{\sigma p}{p}$	w_{final}
D_s + Tracks	0.38	48 μm	0.08	0.13
Lepton + D	0.16	54 μm	0.07	0.04
Charge Dipole	0.12	72 μm	0.07	0.24

Table 5. Performance parameters of the three final state tags.

the decay length is calculated. Figure 25 shows the reconstructed mass distribution of the D_s candidates, and a clear D_s signal is seen.

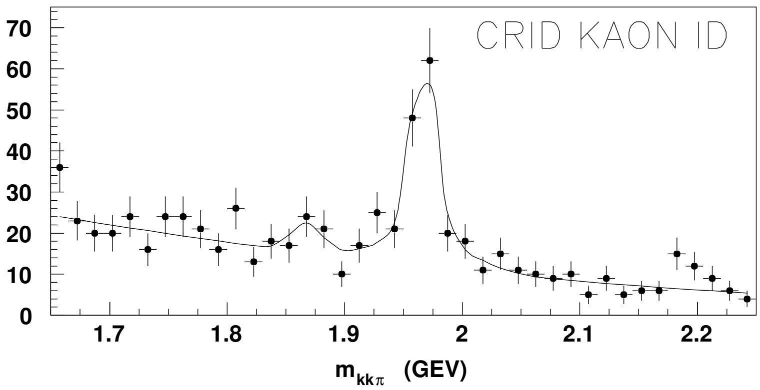

Fig. 25. Plot of the three body mass $m_{KK\pi}$ for D_s candidates. The CRID is used to identify kaons. A clear D_s peak is observed.

7.3.2 Lepton + D

In the "Lepton + D" method, a Neural Network similar to the one used for the A_b measurement (section 5.4.1) is used to select neutral semi-leptonic B decays. This network is also used to suppress "wrong sign" leptons from cascade $b \to c \to \bar{l}$ decays. The tag also requires a separate topologically reconstructed D vertex. The B decay point is then reconstructed by vertexing the lepton with the tracks from the D vertex.

7.3.3 Charge Dipole

The last final state tag is the fully inclusive "Charge Dipole" technique. As shown in Figure 26 this technique exploits the $b \to c$ decay topology of B_s decays. For a B_s decay, the tracks coming from the b decay vertex can have a charge of either 0 or 1, while the tracks coming the cascade c decay can have a charge of either -1 or 0. For $\bar{B}_s$ decays the situation is reversed. Due to SLD's excellent vertex resolution, the b and c vertices can often be distinguished topologically. The measured distance between the vertices is L and the "charge dipole" is defined as $\delta q = (Q_D - Q_B) \times L$. So, for $\delta q > 0$, it is likely the decay was a $\bar{B}_s^0$. And, for $\delta q < 0$, it is likely that the decay was a B_s^0. Figure 27 shows the separation provided by the dipole.

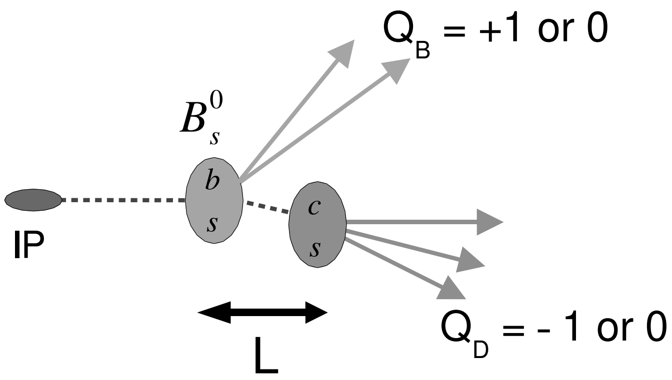

Fig. 26. Illustration the "dipole" technique for final state tagging.

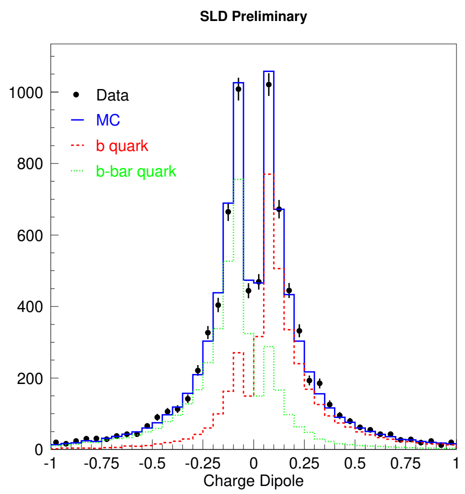

Fig. 27. Distribution of the quantity δq, as defined in the text. There is good separation between b and $\bar{b}$.

7.4 Amplitude Fit Method

In order to extract a signal (or limit) for B_s^0 mixing, the so-called "Amplitude Fit" method is used.[14] In this method the probability for mixing as a function of time is fitted to the expressions

$$Prob(B_s^0 \to B_s^0) = \frac{1}{2}\Gamma e^{-\Gamma t}(1 + Acos\Delta m_s t) \quad (25)$$

$$Prob(B_s^0 \to \bar{B}_s^0) = \frac{1}{2}\Gamma e^{-\Gamma t}(1 - Acos\Delta m_s t), \quad (26)$$

where Γ is the decay width and A is the mixing amplitude, which is the free parameter in the fit. As we scan through all possible values of Δm_s, we would expect $A = 1$ for the true value Δm_s and $A = 0$ for Δm_s away from the true value. One can think of this method as a "Fourier Transform" of the data. Figure 28 shows the results of this fit for a large Monte Carlo sample of Lepton + D events.

To set a 95% confidence limit on Δm_s we find those values of A for which $A + 1.65\sigma_a < 1$. To determine the "Sensitivity", which is the expected limit if the experiment were repeated many times, we find those values of A for which $1.65\sigma_A < 1$.

Perhaps the most important advantage of this method is that it allows the combination of several samples, such as from different final state tags, or from different experiments. Figure 29 shows the SLD amplitude fit results for the combination of all three final state tags. Based on this fit, SLD excludes at 95% confidence level the region $\Delta m_s < 7.6$ ps^{-1} and the region $11.8 < \Delta m_s < 14.8$ ps^{-1}.

7.5 B_s Mixing World Average

SLD's amplitude fits can also be combined with those of the rest of the world. Figure 30 shows this world average as of Summer 2000. SLD's data is especially important at high Δm_s, due to the excellent σ_t resolution. The sensitivity of the world average is 17.9 ps^{-1} and it is able to rule out the region $\Delta m_s < 14.9$ ps^{-1}.

8 Conclusion

The SLD physics program has made large contributions in the areas of electroweak, QCD and heavy flavor Physics at the Z^0. Table 6 lists some highlights of this program. In addition to these measurements, SLD also has many other interesting results for which there was not space in this paper.

References

[1] SLD Collaboration, K. Abe *et al.*, *Phys. Rev.* D **53**, 1023 (1996).

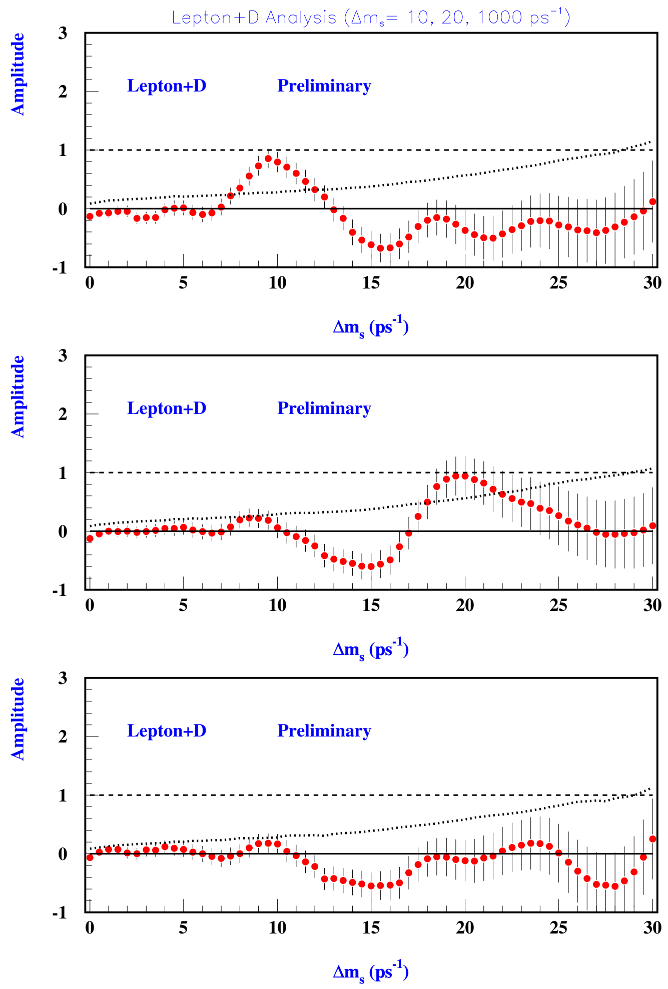

Fig. 28. Monte Carlo demonstration of the Amplitude Fit method for a sample of lepton + D decays. In the top plot, the data was generated with $\Delta m_s = 10$ ps^{-1} and a clear signal is observed there. In the middle plot, $\Delta m_s = 20$ ps^{-1} was used and a somewhat less significant signal is observed. In the bottom plot, $\Delta m_s = 1000$ ps^{-1} was used, which is beyond the sensitivity of the analysis and no signal is observed.

[2] SLD Collaboration, K. Abe *et al.*, *Phys. Rev. Let.* **85**, 5059 (2000).

[3] SLD Collaboration, K. Abe *et al.*, *Phys. Rev. Let.* **86**, 1162 (2001).

[4] D.J. Jackson, *Nucl. Instr. & Meth.* **A86**, 1162 (1997).

[5] The LEP Electroweak Working Group, EP Preprint Summer 2000, CERN-EP/2001-021.

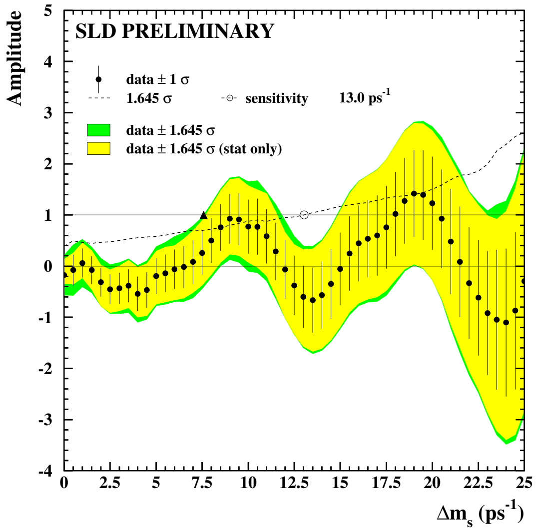

Fig. 29. Combined amplitude fit for the three final state tags.

Measurement	Value
A^0_{LR}	$0.15138 \pm 0.00216 \Rightarrow \boldsymbol{\sin^2\theta_w^{eff} = 0.23097 \pm 0.00027}$
R_b	$0.21669 \pm 0.00094 \pm 0.00101$
$\boldsymbol{R_c}$	$\boldsymbol{0.1732 \pm 0.0041 \pm 0.0025}$
A_b	0.914 ± 0.024
A_c	0.635 ± 0.027
$\boldsymbol{A_s}$	$\boldsymbol{0.895 \pm 0.066 \pm 0.062}$
$\boldsymbol{\langle x_B \rangle}$	$\boldsymbol{0.709 \pm 0.003 \pm 0.005}$
Δm_s	Exclude $\Delta m_s < 7.6$ ps^{-1} and $11.8 < \Delta m_s < 14.8$ ps^{-1}

Table 6. Table summarizing the results presented in this paper. Those that are the world's best are indicated in bold.

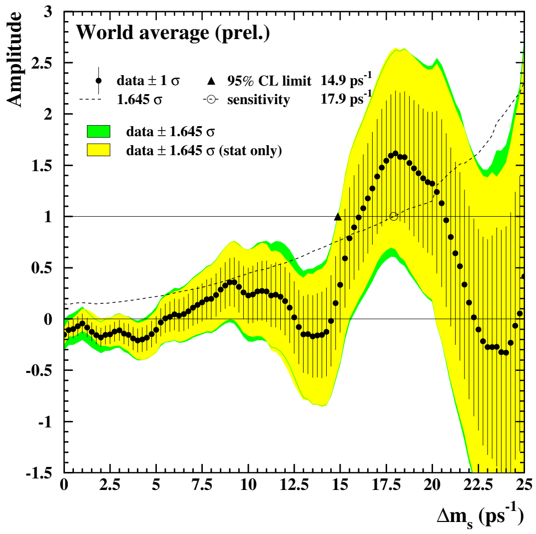

Fig. 30. Combined amplitude fit for the world's B_s mixing data as of Summer 2000.

[6] SLD Collaboration, K. Abe *et al.*, *"Direct Measurement of A_b at the Z^0 Pole Using a Lepton Tag*, SLAC-PUB-8516 (2000) [hep-ex/0009064].

[7] SLD Collaboration, K. Abe *et al.*, *"Direct Measurement of A_b Using Charged Vertices"*, SLAC-PUB-8542 (2000).

[8] SLD Collaboration, K. Abe *et al.*, *Phys. Rev.* D **63**, 032005 (2001).

[9] SLD Collaboration, K. Abe *et al.*, *Phys. Rev. Let.* **85**, 5059 (2000).

[10] SLD Collaboration, K. Abe *et al.*, *Phys. Rev. Let.* **84**, 4300 (2000).

[11] T. Sjostrand, Computer Physics Commun. **82**, 74 (1994).

[12] A. Hoecker and V. Kartvelishvili, NIM **A372**, 469 (1996).

[13] S. Mele, *Phys. Rev.* D **59**, 113011 (1999).

[14] H.-G. Moser and A. Roussarie, *Nucl. Instr. & Meth.* **A384**, 491 (1997).